ISSN: 2096-3246
Volume 55, Issue 01, January, 2023

Geochemistry and mineralogy of oil shale from Attarat Umm Ghudran area, Jordan

Khalil M. Ibrahim[1*], Hanan Abdel Rahman[1]

Department of Earth and Environmental Sciences, Prince El-Hassan bin Talal Faculty of Natural Resources and Environment, The Hashemite University, P.O. Box 330127, Zarqa 13133, Jordan[1]

Corresponding author: 1*

Keywords:
Oil shale; Attarat Umm Ghudran; geochemistry; trace elements; Jordan; cluster analysis.

ABSTRACT

Commercial oil shale is widespread in Jordan occurring mostly in the subsurface. More than 20 localities were reported including Attarat Umm Ghudran (AUM) area. Selected oil shale boreholes drilled in the AUM were sampled, analysed and studied in detail. The purpose is to verify their mineralogical composition and geochemical affinities including trace elements content. They were characterized using the polarizing microscopic, X-ray diffraction (XRD), scanning electron microscopy, and X-ray fluorescence spectrometry. Petrographically, the studied oil shale consists of bioclastic mudstone-wackestone, bioclastic packstone and foraminiferal grainstone. The XRD indicates that calcite is the dominant mineral with subordinate quartz. This was emphasized by chemical analysis. The average CaO is 31.03 wt.% followed by SiO_2 which makes an average of 16.7 wt.%. The average content of SO_3, Al_2O_3 and P_2O_5 is 2.69%, 2.25% and 2.1% respectively. Cluster analysis and correlation matrix were calculated for the major and trace element. The cluster analysis subdivided the elements into three group; including a carbonate group, an aluminosilicate group and a phosphate-sulfide group. In general, the studied oil shale is enriched in Zn, Sr, Cr, V, Ni, Zr, Cu, Mn, Rb and U. Uranium attains an average concentration of 21.15 ppm. Chemical composition results were compared with other localities. It was concluded that the enrichment is the result of the euxinic depositional environment, where they would co-precipitate mainly as sulfide minerals. The heavy metals in the oil shale are redox sensitive elements and are related to Mississippi Valley-type deposits.

1. INTRODUCTION

Oil shale is a sedimentary rock containing varying amounts of kerogen that produces significant quantities of shale oil when heated to high temperatures, which was classified oil shale into three groups based upon their environment of deposition [1]. Marine oil shale is one of these groups, which consist of tasmanite and marinite. In general, the mineral composition of oil shale is carbonate, including calcite, with lesser amounts of aluminosilicate minerals [2]. Oil shale is often enriched with heavy metals such As, Cd, Mn, Mo, Se, Cr, Zn, Ni and V [3], [4].

Jordan now is ranked as the world's fourth country with its oil shale resource. The oil shale in Jordan was reported in more than 20 localities [5]. It is marinite type deposited during the Late Cretaceous to Early Eocene [6]. The organic matter of the Jordanian oil shale is amorphous kerogen, which has been produced from marine planktonic organisms by bacterial degradation, and the product of its fossilization. Attarat Umm Ghudran (AUG) is an important locality among the three major deposits occurring in central Jordan (Figure 1) [7].

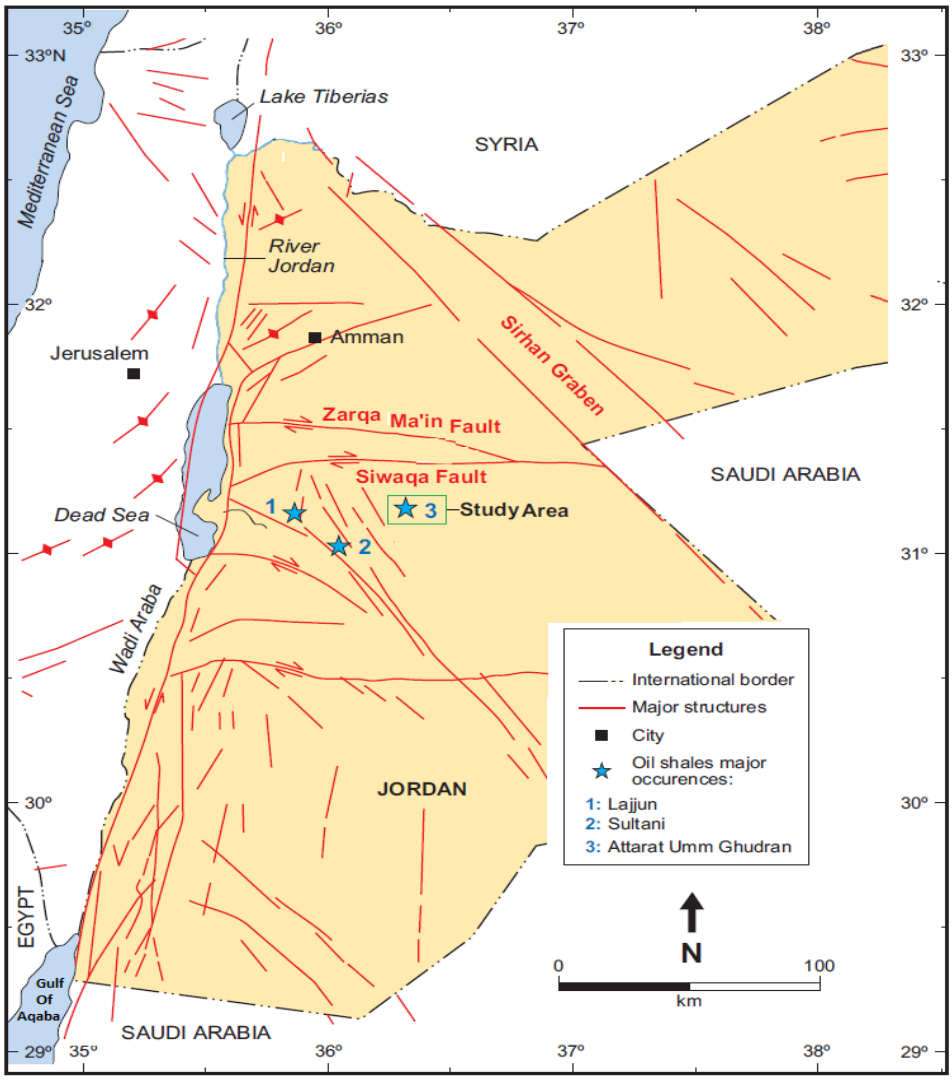

Figure 1. Location map of major oil shale deposits in central Jordan [5]

1.1 Geological setting

The AUG oil shale deposit is located in central Jordan, about 70 km south of Amman (Figure 1). The expected area of the whole AUG oil shale deposit is about 200 km^2. The geological setting of central Jordan is dominated by widespread deposition of thick marine carbonates and associated lithologies represented by the Late Cretaceous- Paleogene Balqa' Group [8]. The sedimentation during that time interval took place on a broad, shallow shelf that covered the northern edge of the Arabian Plate [8]. Central Jordan is faulted and transacted by the Swiaqa Faults system (Figure 1), which is an EW-trending strike-slip fault with a dextral movement [9].

The AUG oil shale is mainly marly limestone to chalky marl in which the organic matter is finely dispersed

in the rock [10]. The oil shale is rather homogenous grey-, black-, brownish- grey-colored succession of laminated kerogen-bearing carbonate rocks [11]. As summarized in Table 1, thickness of the oil shale within the study area varies from 23 m to about 46.5 m. The oil shale occurs in the subsurface, where the overburden is between 61 m and 88.5 m.

Table 1. Borehole data.

Borehole	Thickness (m)			Total depth (m)
	Overburden	Oil shale	AHP[1]	
QC-30	88.5	46.5	10	145
QC-01	61	35	6	102
QC-02	70	30	2	102
QC-03	88	23	3	114
QC-04	64	36	3	103
QC-05	67	33	3	103
QC-22	61	37	2	100

[1]AHP: Al Hasa Phosphorite Formation, underlaying unit.

The AUG area is under thorough and detailed exploration work [12]. In the western part of the AUG oil shale deposit, the Al- Qamar for Energy and Infrastructure Ltd. Co. (QEI) was assigned 64 km^2 area to conduct an exploration program. Therefore, a drilling campaign was conducted to study the subsurface geology including overburden thickness and distribution, oil shale thickness and distribution. Seven boreholes were used in this study as in Table 1.

2. Materials and Methods

Thirty core samples of the oil shale from the seven boreholes were provided by the QEI. Oil shale samples were crushed and pulverized to the desired size in the laboratories of the Hashemite University. The samples have been subjected to different kinds of testing and analyses following the standard methods [13].

The XRF was used to measure major (wt. %) and trace (ppm) elemental concentrations directly from samples. Thus, pressed powder pellet technology was used for the whole range of elements. The XRF analysis was conducted at the Jordan Atomic Energy Commission with the S4 Pioneer Spectrometer (Bruker AXS GmbH), using an X-ray tube with a rhodium anode, which operated with a power of 3 kW. Loss on ignition was determined from 1 g of sample material at 920 °C. The petrography and mineralogy were determined using polarizing microscope, scanning electron microscope SEM-EDX and powder X-ray diffraction (XRD).

[14], [15] classifications were used in the petrographical studies. Microfacies types for the studied thin sections were compared with standard microfacies zones to determine the depositional environment [16].

For the petrographic study, representative number of thin sections were prepared using standard methods. Half of each thin section was stained with the Alizarin Red Solution (ARS), and the whole section was stained with blue dye. The microscopic investigation and imaging have been performed using a Nikon ECLIPSE LV100POL polarising light microscope attached with a Nikon DS-Ri2 camera to examine the mineral composition, lithofacies and diagenetic features.

The morphology of oil shale was examined by scanning electron microscopy using model Quanta 600, FEI SEM. The XRD analysis was carried out on the same samples at the Hashemite University labs. This technique allows the determination of the mineral constituents, using Shimadzu X-ray diffractometer

(MAXima XRD-7000) equipped with a Cu-target tube and a curved graphite monochromator. The XRD pattern was recorded over a 2-theta interval of 5–40 degree.

Geochemical data were presented as colored maps within the ArcGIS software by converting and digitizing and georeferencing the study area map to raster data, then geostatistical tools (kriging and natural neighbour) were used to create distribution map for the analysed components. The concentration was represented as color codes and contour line. Statistical method was used to generate scatter plots and carry out correlation matrix and cluster analysis. The statistical significance was computed using XLSTAT 2018 software.

3. Results and Discussion

3.1 Petrography

Petrographic investigation indicates that the oil shale samples are made of different types of clasts embedded in organic matter-rich carbonate matrix and calcite cement. The microcrystalline calcite matrix "micrite" is prevalent in all thin sections. Clasts in the Eocene oil shales from Jordan were subdivided into skeletal and non-skeletal types [6]. This seems applicable for the AUG oil shale. The content of skeletal and non-skeletal clasts in the studied thin sections range from 10% to 40%, mainly composed of calcite and organic matter filling pore space in addition to authigenic quartz, phosphate and opaque minerals. This result resembles that reported by previous works which indicated skeleton debris between 10–50% [11].

In the studied samples, skeletal fossil fragments include mainly benthic and planktonic foraminifera microfossils (Figure 2). The non-skeletal grains include pelloids, which are small, sorted, and rounded clasts made of micrite (Figure 2). Organic matter is the dark brown- to light-brown- colored material confined to the matrix in Figure 2.

The foraminiferal tests and fragments are abundant as illustrated in Figure 2. They vary in sizes from less than 20 micron up to 0.45 mm. Size range for shells from 0.005–0.2 mm, randomly up to 2 mm have been reported. The shell walls composed of microsparite, and the shell chambers are either empty or filled by microsparite or micrite.

Skeletal bone fragments are less abundances. They show elongated and branching shapes, some of them are fractured and with perforations. The bones are composed of apatite. Irregular shape collophane clasts are less abundance. They have colorless-yellowish color in PPL view and are isotropic in XPL view. Apatite clasts are bind together by a massive micrite that is greatly mixed with organic matter and iron oxides forming the matrix of the rock.

In general, samples show massive texture without any sedimentary fabric; the grains are embedded within the matrix without any preferred orientation (Figure 2a, 2b, 2d). However, the rock sometimes exhibits prominent preferred orientation of grains and matrix material in one direction giving the rocks its lamination as in Figure 2.

Based on the microfacies models [17], the studied oil shale samples consist of bioclastic mudstone-wackestone (Figure 2c and 2d), bioclastic packstone (Figure 2b) and foraminiferal grainstone (Figure 2a).

ISSN: 2096-3246
Volume 55, Issue 01, January, 2023

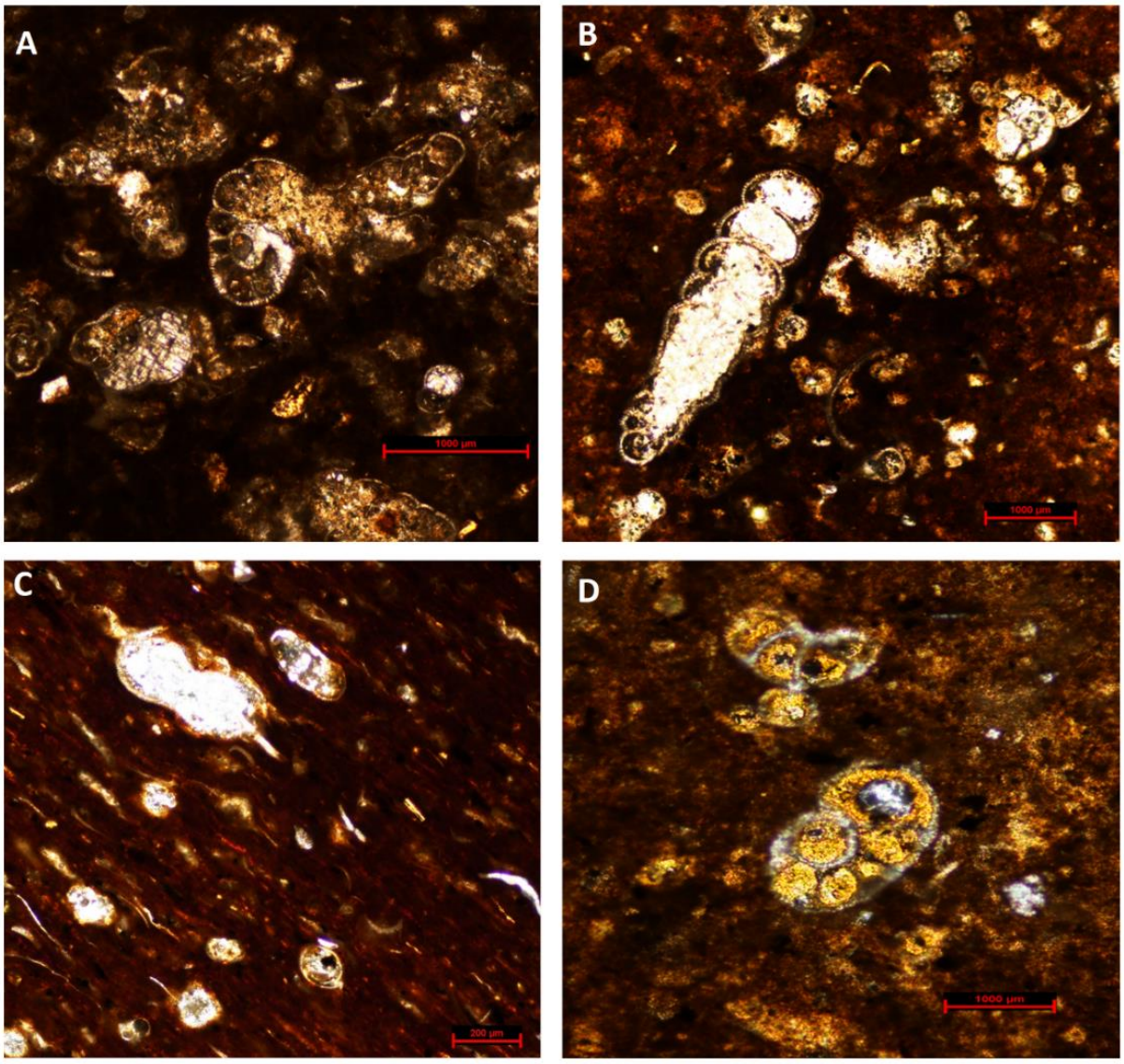

Figure 2. Photomicrographs of the studied oil shale samples shows skeletal fossil fragments consist of benthic and planktonic foraminiferal tests embedded in the organic matter matrix.

3.2 Mineralogy

XRD results indicate that the mineralogy of the AUM oil shale is uniform in all boreholes. Calcite is the primary component exists in all samples (Figure 3). The oil shale is also rich in the mineral quartz. Minor minerals include apatite and clay minerals. Dolomite has also been found in some of the oil shale samples at specific intervals. Similar results were reported earlier for the AUG [10], [11].

Results of the SEM-EDX is shown Figure 4. It clearly indicates presence of predominant carbonate phase in form of calcite with CaO =47.97 % followed by silica (10.04 %) mainly as free silica, sulfate/sulfide phase (SO_3 = 7.31 %), phosphate (P_2O_3 = 1.9 %) and clays (Al_2O_3 = 1.1 %). The organic matter rich matrix is abundant with dark tones and massive texture. The organic matter rich matrix is abundant with dark tones and massive texture. The morphology shows wide range in particle size, the crystal habit exhibits moderate roundness and low sphericity.

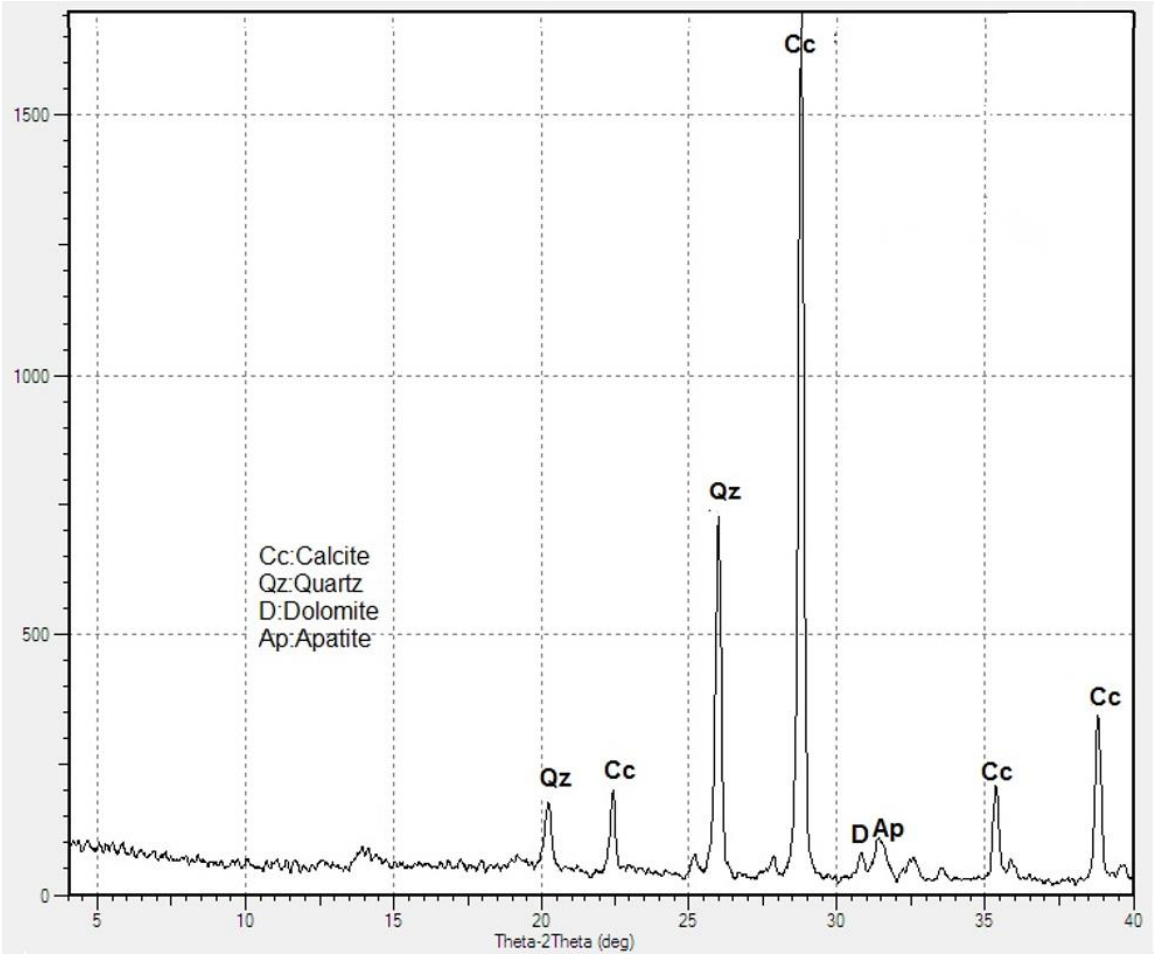

Figure 3. X-ray diffractogram of the oil shale.

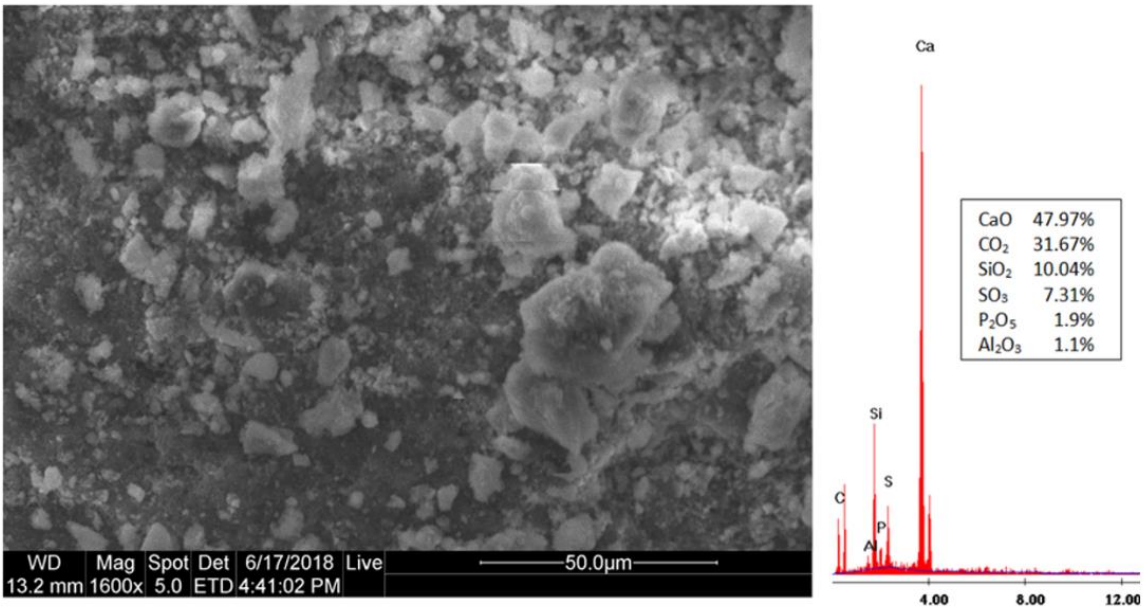

Figure 4. SEM-EDX of the oil shale, shows the main chemical components.

3.3 Statistical Analysis

3.3.1 Cluster analyses

The cluster analysis subdivided the analysed elements into three clusters which are carbonate group; iron-aluminosilicate group; and phosphate-sulfide group. The dendrogram which shows dissimilarities percentage among elements in the geochemical data is illustrated in Figure 5. The carbonate group (CaO-Sr, Th-Y, Mn-Rb, and Ba) has > 60% similarity compared with the >72 similarity in the iron-aluminosilicate cluster (SiO_2, Al_2O_3, Na_2O, K_2O, MgO, TiO_2, Fe_2O_3, Cr and Cu); and > 68 similarity in the phosphate-sulfide cluster (P_2O_5, SO_3, V, Zn, U, Ni and Zr).

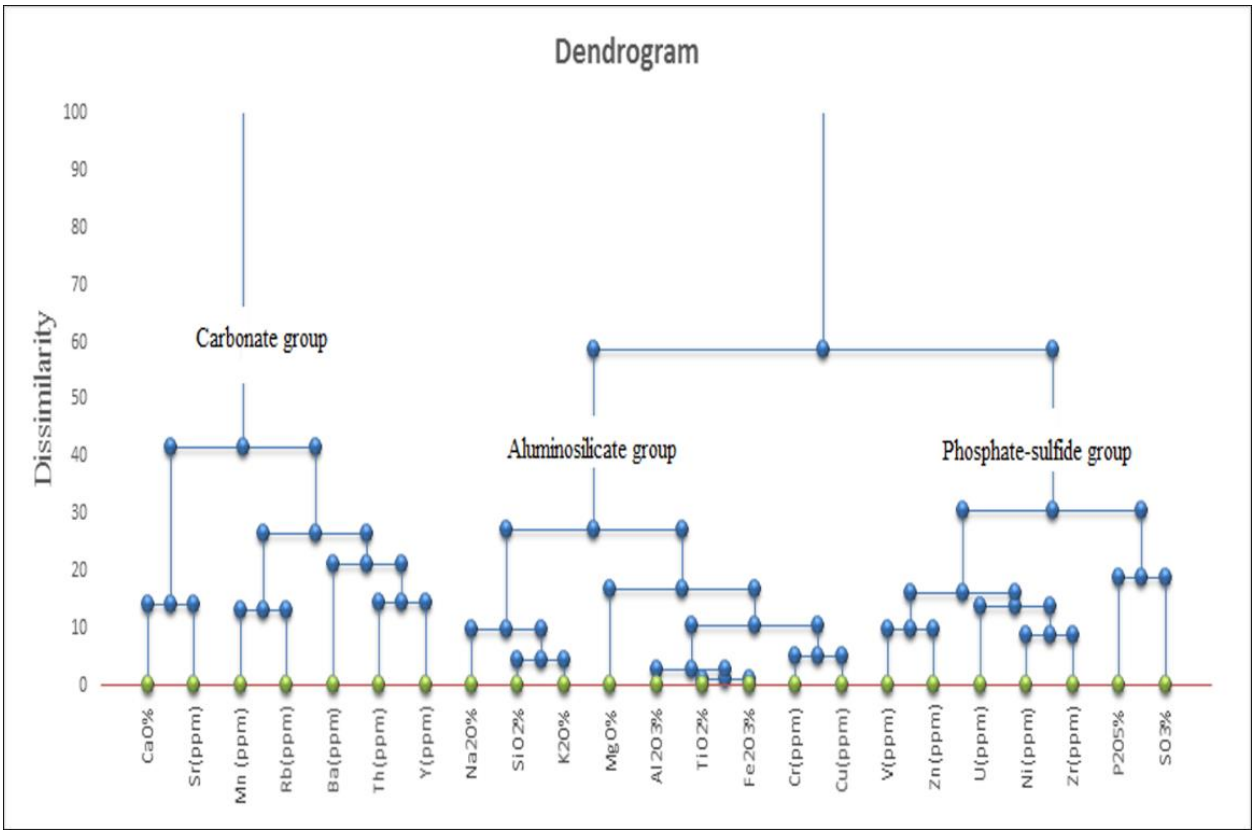

Figure 5. Dendrogram shows results of cluster analysis.

In details, within the carbonate cluster, CaO and Sr are strongly associated at 86% similarity, but the Mn - Rb remains the strongest association at 87% similarity, whereas 85% similarity is between Th and Y. And 80% similarity is between (Th, Y) and Ba. The close association of the said elements with Ca is most probably due to incorporation within the carbonate mineral phases. Either substituting Ca within calcite or forming their own carbonate minerals. Sr in sedimentary rocks is predominantly found in carbonate rocks composed of calcite, aragonite and/or dolomite [18]. It was indicated that Sr can replace Ca in any proportion and there is a continuous solid-solution series [19]. Whereas for Mn is absorbed by marine algae, with subsequent organic decay in the sediment producing alkaline and reducing porewaters that may have resulted in formation of $MnCO_3$ [20]. The Mn-carbonate (rhodochrosite) interbedded with Mn-bearing shale, both having a high organic carbon content and abundant pyrite was reported elsewhere [21].

Within the Fe-aluminosilicate cluster, Fe_2O_3 shows almost the strongest similarity with TiO_2 at 99%. This is followed by Fe_2O_3-TiO_2 with Al_2O_3 at 97% similarity, and by Cr with Cu at similarity 95%. On the other hand, a strong similarity is noted between SiO_2 and K_2O equal to 95%, followed by SiO_2 - K_2O and Na_2O with a similarity of 90%. They most probably originate from clay minerals, which are also supported by the occurrence of kaolinite and illite [22]. In Al Lajjun oil shale area, elements clustered in the Al-group were

conceded as detrital elements, whereas the non-Al group elements were considered as hydrogenous elements [38].

The similarity of P_2O_5 with SO_3 is 80%. Within this group the highest similarity is between Ni and Zr reach 90%, followed by between V and Zn at 89% and between Ni -Zr and U at 85%. All those trace elements are normally related to phosphate-sulfide group.

3.3.2 Correlation coefficient matrix

A correlation matrix was calculated for the major and trace element. The correlation coefficient matrix is shown in Figure 6. SiO_2 shows strongly negative correlation with CaO (r = -0.9), but it shows strongly positive correlation with K_2O (r = 0.85). Further SiO_2 exhibits good correlation with Na_2O (r = 0.7), Al_2O_3 (r = 0.69), TiO_2 (r = 0.65), and Zr (r = 0.64).

In addition to SiO_2, CaO also is negatively correlated with many elements including K_2O (r = -0.8), Al_2O_3 (r = -0.77), Cr (r = -0.78), TiO_2 (r = -0.747), Fe_2O_3 (r = -0.67), and Zr (r = -0.64). Al_2O_3 shows strongly positive correlation with TiO_2, Fe_2O_3 and Cr (r = 0.94, 0.91 and 0.83) respectively. And positive correlations exist between Al_2O_3- MgO (r = 0.67) and Cu (r =.0.67). Fe_2O_3 shows strongly positive correlation with TiO2 (r = 0.97) and Cr(r = 0.85), also good correlation is between Fe_2O_3 - Cu (r = 0.79), Fe_2O_3 - MgO (r = 0.66), and Fe_2O_3 - Mn (r = 0.65). Positive correlation is evident between K_2O and each of Al_2O_3 (r = 0.85), TiO_2 (r = 0.83), Fe_2O_3 (r = 0.77), Cr (r = 0.71), Na_2O (r = 0.72), MgO (r = 0.64), Zr (r = 0.65).

Variables	Na2O%	Al2O3%	SiO2%	P2O5%	K2O%	CaO%	TiO2%	Fe2O3%	SO3%	MgO%	U(ppm)	V(ppm)	Cr(ppm)	Mn (ppm	Ni(ppm)	Cu(ppm)	Zn(ppm)	Rb(ppm)	Sr(ppm)	Y(ppm)	Zr(ppm)	Ba(ppm)
Na2O%	1.00	0.52	0.70	0.33	0.72	-0.73	0.59	0.51	0.34	0.36	0.47	0.55	0.59	0.18	0.51	0.37	0.40	-0.19	-0.37	-0.30	0.63	0.04
Al2O3%		1.00	0.69	0.12	0.85	-0.77	0.94	0.91	0.10	0.67	0.29	0.45	0.83	0.38	0.42	0.67	0.27	0.08	-0.17	-0.03	0.56	0.42
SiO2%			1.00	0.27	0.85	-0.90	0.65	0.55	0.13	0.55	0.34	0.43	0.53	0.04	0.27	0.30	0.35	-0.21	-0.59	-0.05	0.64	0.31
P2O5%				1.00	0.25	-0.34	0.09	0.07	0.35	-0.14	0.41	0.25	0.22	-0.22	0.10	0.22	0.22	-0.28	-0.29	-0.11	0.12	0.07
K2O%					1.00	-0.80	0.83	0.77	0.07	0.64	0.43	0.52	0.71	0.25	0.39	0.43	0.29	0.02	-0.39	-0.08	0.65	0.36
CaO%						1.00	-0.74	-0.67	-0.41	-0.48	-0.49	-0.59	-0.77	-0.15	-0.47	-0.59	-0.57	0.28	0.52	0.14	-0.64	-0.38
TiO2%							1.00	0.97	0.07	0.72	0.28	0.49	0.86	0.53	0.48	0.72	0.39	0.26	-0.20	0.00	0.56	0.42
Fe2O3%								1.00	0.09	0.66	0.22	0.54	0.85	0.65	0.47	0.79	0.40	0.34	-0.08	0.05	0.50	0.46
SO3%									1.00	-0.21	0.34	0.46	0.41	-0.07	0.40	0.39	0.42	-0.31	-0.05	-0.59	0.27	0.00
MgO%										1.00	0.07	0.24	0.50	0.47	0.23	0.36	0.06	0.25	-0.38	0.03	0.39	0.29
U(ppm)											1.00	0.56	0.49	-0.02	0.60	0.26	0.42	-0.24	-0.44	-0.05	0.54	0.31
V(ppm)												1.00	0.56	0.37	0.64	0.56	0.66	0.01	-0.16	-0.16	0.58	0.30
Cr(ppm)													1.00	0.40	0.66	0.82	0.55	0.05	-0.15	-0.16	0.59	0.43
Mn (ppm)														1.00	0.20	0.53	0.20	0.55	0.16	0.15	0.07	0.36
Ni(ppm)															1.00	0.62	0.66	-0.01	-0.24	-0.21	0.70	0.34
Cu(ppm)																1.00	0.67	0.13	-0.01	0.02	0.39	0.51
Zn(ppm)																	1.00	-0.03	-0.24	0.03	0.47	0.42
Rb(ppm)																		1.00	0.32	0.15	-0.13	0.13
Sr(ppm)																			1.00	0.01	-0.39	-0.21
Y(ppm)																				1.00	-0.07	0.15
Zr(ppm)																					1.00	0.26
Ba(ppm)																						1.00

Figure 6. Correlation coefficient matrix of the major, minor trace elements.

3.4 Geochemistry of major oxides

3.4.1 CaO

The first most abundant element in the studied AUG oil shale samples is CaO. As it can be noted in Table 2, the oil shale has an average CaO equal to 31.03%. It is slightly higher than the average CaO reported for the oil shale deposits in al Lajjun and Sultani areas as in Table 3 [38], [39]. However, it is still lower than the average CaO reported earlier from AUG oil shale [7], [10]. The spatial distribution of the average CaO in the study area is shown in Figure 7A. High concentrations of average CaO content are observed in the north and northwest. It decreases southwards. The central area shows low to moderate concentrations. Vertical variation in CaO content is minimal apart from cases reported in few boreholes.

Table 2. Summary statistics of the chemical analysis of the studied oil shale samples.

Major Oxides (%)	Minimum	Maximum	Mean	Std. deviation
CaO	17.54	50.46	31.03	7.72
SiO_2	4.43	35.86	16.75	7.63
Al_2O_3	0.59	4.04	2.25	0.97
SO_3	0.82	5.67	2.69	0.95
P_2O_5	0.64	5.00	2.12	0.94
Fe_2O_3	0.32	1.97	0.96	0.40
MgO	0.33	0.85	0.55	0.14
Na_2O	0.05	1.00	0.29	0.20
K_2O	0.01	0.57	0.17	0.17
TiO_2	0.03	0.27	0.12	0.06
LOI	35.30	48.03	42.66	
Trace Elements (ppm)				
Zn	307	2180	1105	480.72
Sr	499	1149	786	145.57
Cr	247	611	406	92.57
V	125	847	390	194.53
Ni	119	374	235	58.95
Cu	96	186	141	22.75
Zr	12	258	91	86.72
Rb	12	267	58	55.24
Mn	10	190	46	43.34
Ba	12	163	45	40.08
U	12	34	21	5.16

Binary diagrams in Figure 8 illustrate the relationship between CaO and other major oxides. CaO shows inverse relationship with K_2O, SiO_2, Al_2O_3 and Fe_2O_3. This may indicate that CaO is incorporated in a phase not related to any of these elements. The main source of CaO is calcite with subordinate occurrences of dolomite, apatite and gypsum as confirmed by the XRD results and the petrographic study. Some minerals may exist in the oil shale samples such as siderite ($FeCO_3$) [24], which is the common ferruginous sedimentary mineral. CaO is considered to be dominantly of biochemical origin, while SiO_2, Al_2O_3, TiO_2 and K_2O are attributed to terrigenous origin [26]. CaO may be used as marine indicator because marine oil shale often has considerably more calcium than non-marine ones [27].

Table 3. Summary statistics of the chemical analysis of the studied oil shale samples.

Major Oxides (%)	AUG[1]	AUG[2]	AUG[3]	Sultani[4]	Al Lajjun[4]	Al Lajjun[5]
CaO	31.03	33.91	33.57	26.30	30.43	29.61
SiO_2	16.75	18.90	20.63	26.26	16.13	14.51
Al_2O_3	2.25	2.02	2.06	2.87	3.77	3.44

SO_3	2.69	2.68	2.7	4.38	4.83	4.06
P_2O_5	2.12	2.82	2.99	3.48	3.30	2.65
Fe_2O_3	0.96	0.63	0.65	1.12	1.55	1.50
MgO	0.55	1.37	0.71	0.95	0.65	0.44
Na_2O	0.29	-	0.19	0.27	0.10	0.16
K_2O	0.17	0.25	0.26	1.37	-	0.41
TiO_2	0.12	0.08	0.08	0.13	0.16	-
LOI	42.66	-	35.65	33.00	38.13	42.58
Trace Elements (ppm)						
Zn	307	2180	1105			480.72
Sr	499	1149	786			145.57
Cr	247	611	406			92.57
V	125	847	390			194.53
Ni	119	374	235			58.95
Cu	96	186	141			22.75
Zr	12	258	91			86.72
Rb	12	267	58			55.24
Mn	10	190	46			43.34
Ba	12	163	45			40.08
U	12	34	21			5.16

[1] This study, [2] [10]; [3] [4]; [4] [24]; [5] [23].

Relationship of CaO with some trace elements such as Cr, Zr and Zn shows significant negative correlation (Figure 9). The relationship of CaO with Sr in Figure 9D exhibits a positive correlation. There is a strong probability that mineral strontianite exists in oil shale [25]. The positive correlation between Sr and CaO contents indicate that Sr is controlled mainly by Ca (probably calcite). The results of the cluster analyses indicate that Sr is grouped with CaO (Figure 6).

According to [25], poor negative correlation of CaO with Ba in Figure 6 may indicate poor probability of existing witherite ($BaCO_3$) minerals in the studied sample.

ISSN: 2096-3246
Volume 55, Issue 01, January, 2023

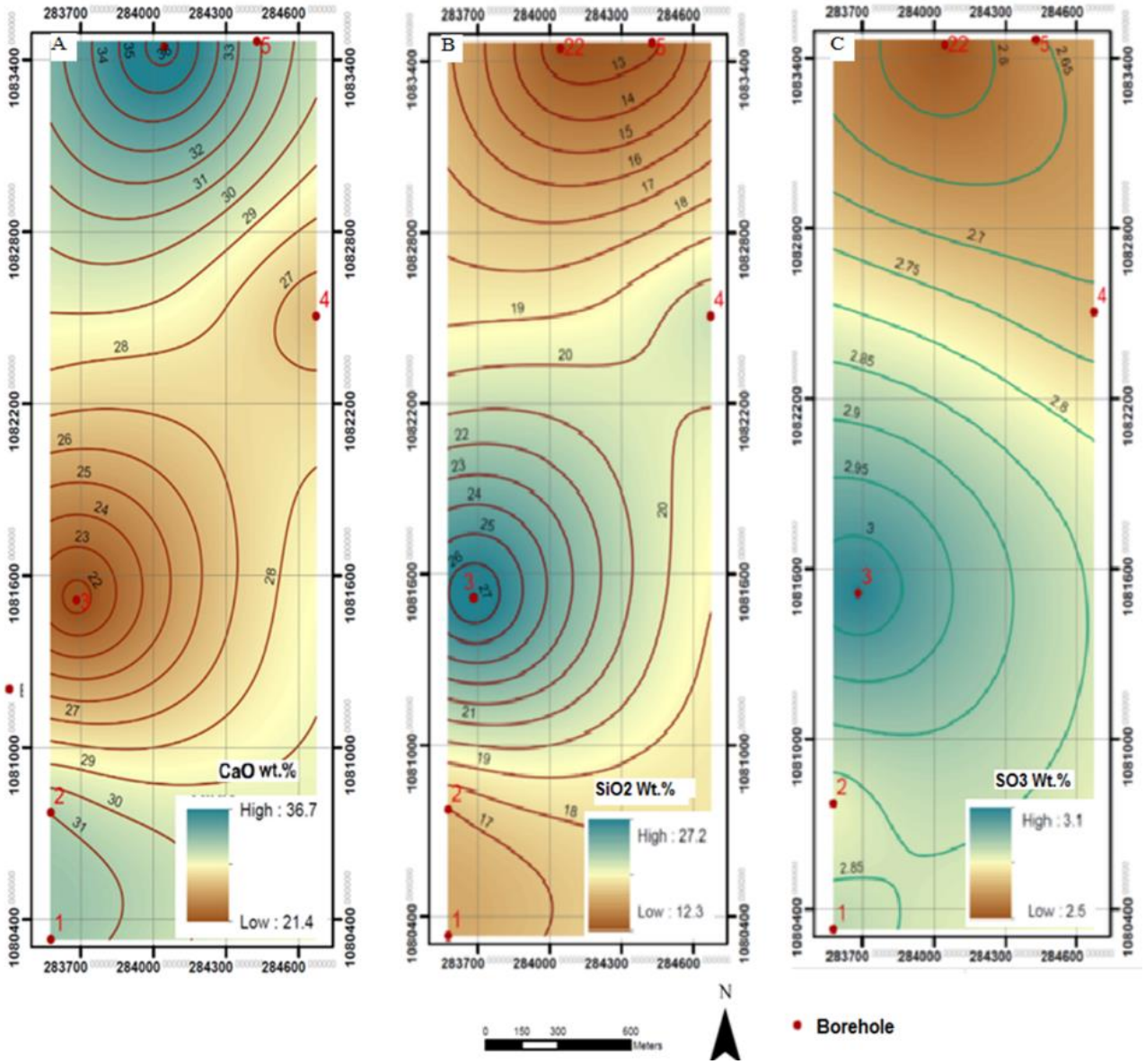

Figure 7. Spatial distribution of selected major oxides in the study area.

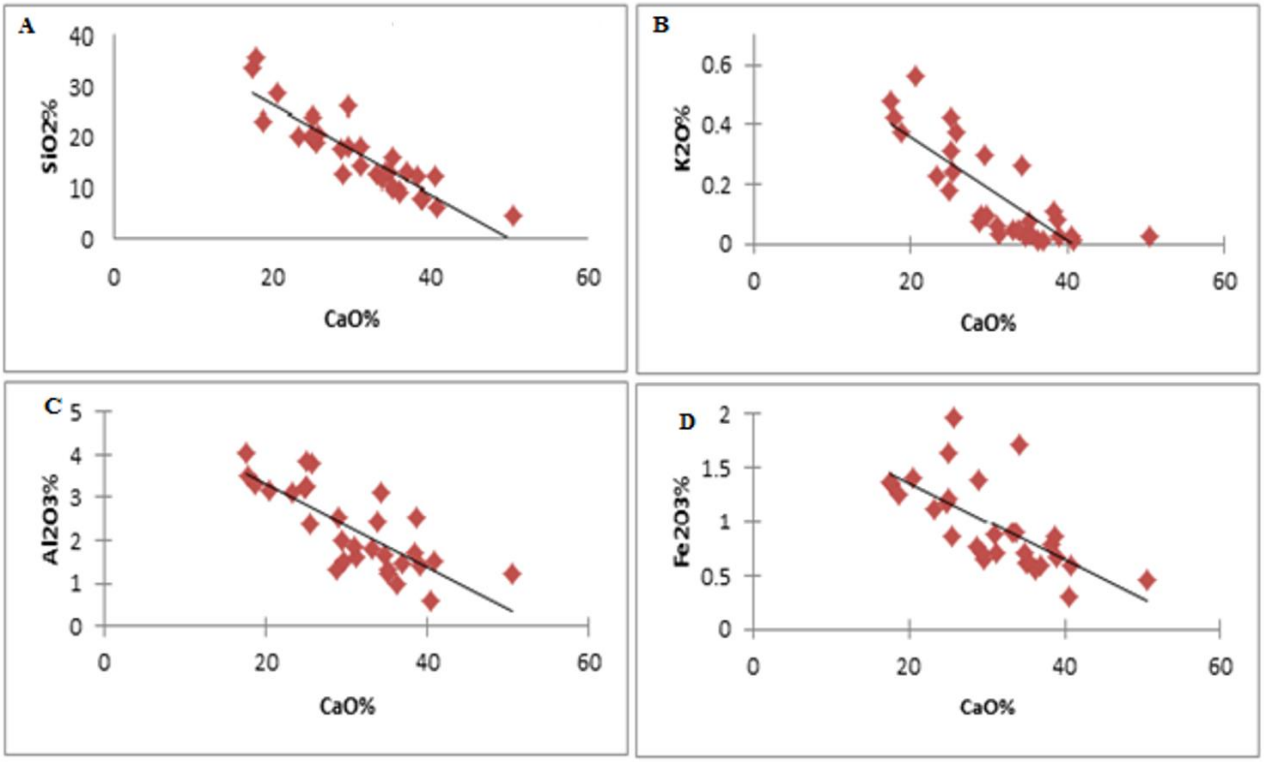

Figure 8. Binary variation diagrams between CaO and selected major oxides.

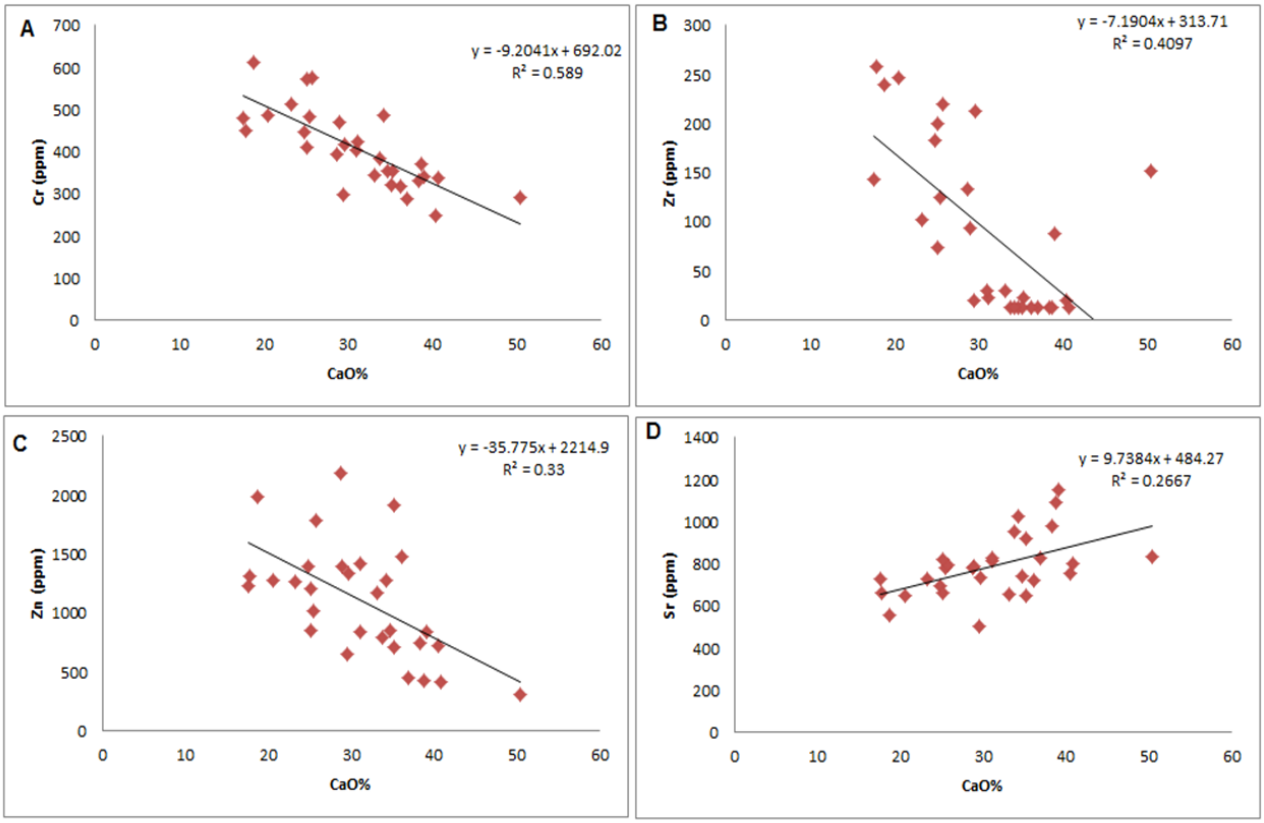

Figure 9. Binary variation diagrams between CaO and selected trace elements.

3.4.2 SiO_2

The second-most abundant component in the studied AUG oil shale samples is silica. The samples exhibit wide variation of SiO_2 content from a minimum value of 4.43% to a maximum value of 35.86%. The average is 16.75% which is close to that reported in Al Lajjun area, but much lower than the average of SiO_2 in Sultani area (26.26%) (Table 2). The spatial distribution of the average SiO_2 content in the study area is displayed in Figure 7B, which indicates that the highest average SiO_2 concentration occurs in the central western part related to borehole No. 3. The vertical variations in SiO_2 content are reported in some boreholes at specific levels. These are related to lithological and mineralogical changes with depth as revealed from borehole logs and petrographic study. Borehole logs indicate presence of free silica in terms of thin porcelanite intervals interbedded with carbonates. This is most probably the cause of high silica content in specific intervals.

Apart from CaO, most major oxides including K_2O, Na_2O, Al_2O_3 and TiO_2, have a proportional linear relationship with SiO_2 contents as in Figure 10. Silica tends to decrease with the increase of carbonates that is primarily controlled by the presence of calcite. The SiO_2 content in the studied oil shale correlates positively with Al_2O_3, this indicates that the SiO_2 is incorporated in the clay minerals [26]. As it is already stated above, porcelanite beds were identified in the boreholes. These beds were incorrectly logged previously as chalk. It was found that the oil shale is not confined to the carbonate phase. It is rather occurring in the porcelanite rich lithology. Free silica may precipitate as cement filling cavities as amorphous silica and later occur as diagenetic quartz distributed with the tiny flakes of the clay minerals or the carbonate mud [28]. This is confirmed by the XRD results. Free silica in form of opal in the oil shale samples was suggested [24].

3.4.3 SO_3

With an average of 2.69 %, SO_3 is the third-most abundant component in the AUG oil shale samples. It varies from a minimum value of 0.82% to a maximum value of 5.67%. It can be concluded that the SO_3 concentration in the AUG oil shale is lower than that reported in Sultani and Al Lajjun oil shale (Table 3).

The spatial distribution of the average SO_3 content is displayed in Figure 7C. Like silica distribution, the highest average SO_3 concentration occurs in the central western part related to borehole No. 3. This is related to the lithological affinities of borehole No. 3 compared with the other boreholes. Wide vertical variations of SO_3 are reported in the boreholes at specific levels. This is most probably related to sulfur content incorporated within the organic matter according to [10].

Cluster analysis indicates that similarity of SO_3 with V, Zn, and Ni is 70% as displayed in Figure 5. Positive correlation is also noticed in Figure 6 with Cu (r=0.39), Cr (r=0.41). Therefore, it can be concluded that one form of SO_3 in the studied oil shale samples is sulfide minerals.

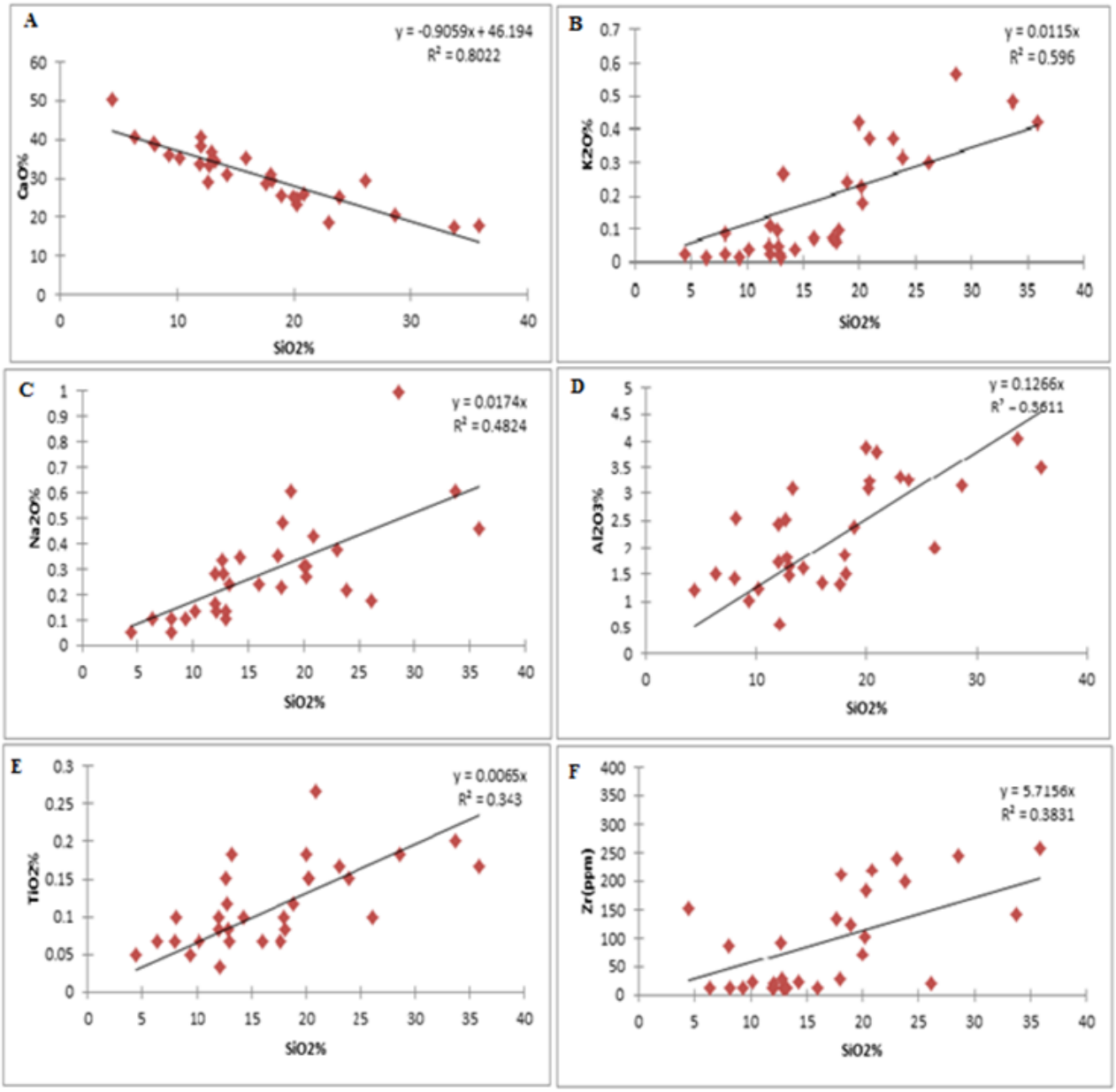

Figure 10. Binary variation diagrams between SiO2 and selected major oxides and Zr.

3.4.4 Al_2O_3

Aluminum is the third most common element in the Earth's crust with 8.1% of the crust's mass. However, in the studied AUG oil shale samples, the Al_2O_3 is the fourth most abundant element (**Error! Reference source not found.**). The average Al_2O_3 in all samples is 2.25% which is lower than the average Al_2O_3 in the Sultani and Al Lajjun oil shale (Table 3).

There variation diagrams which shows the relationship between the Al_2O_3 with major oxide such as TiO_2, Fe_2O_3, SiO_2, MgO, K_2O and CaO is illustrated in Figure 11. Positive relationship exists with TiO_2, Fe_2O_3, SiO_2, MgO and K_2O, whereas negative relationship is noted with CaO. The positive trend might be attributed to terrigenous origin due to the presence of significant amounts of clays [26].

ISSN: 2096-3246
Volume 55, Issue 01, January, 2023

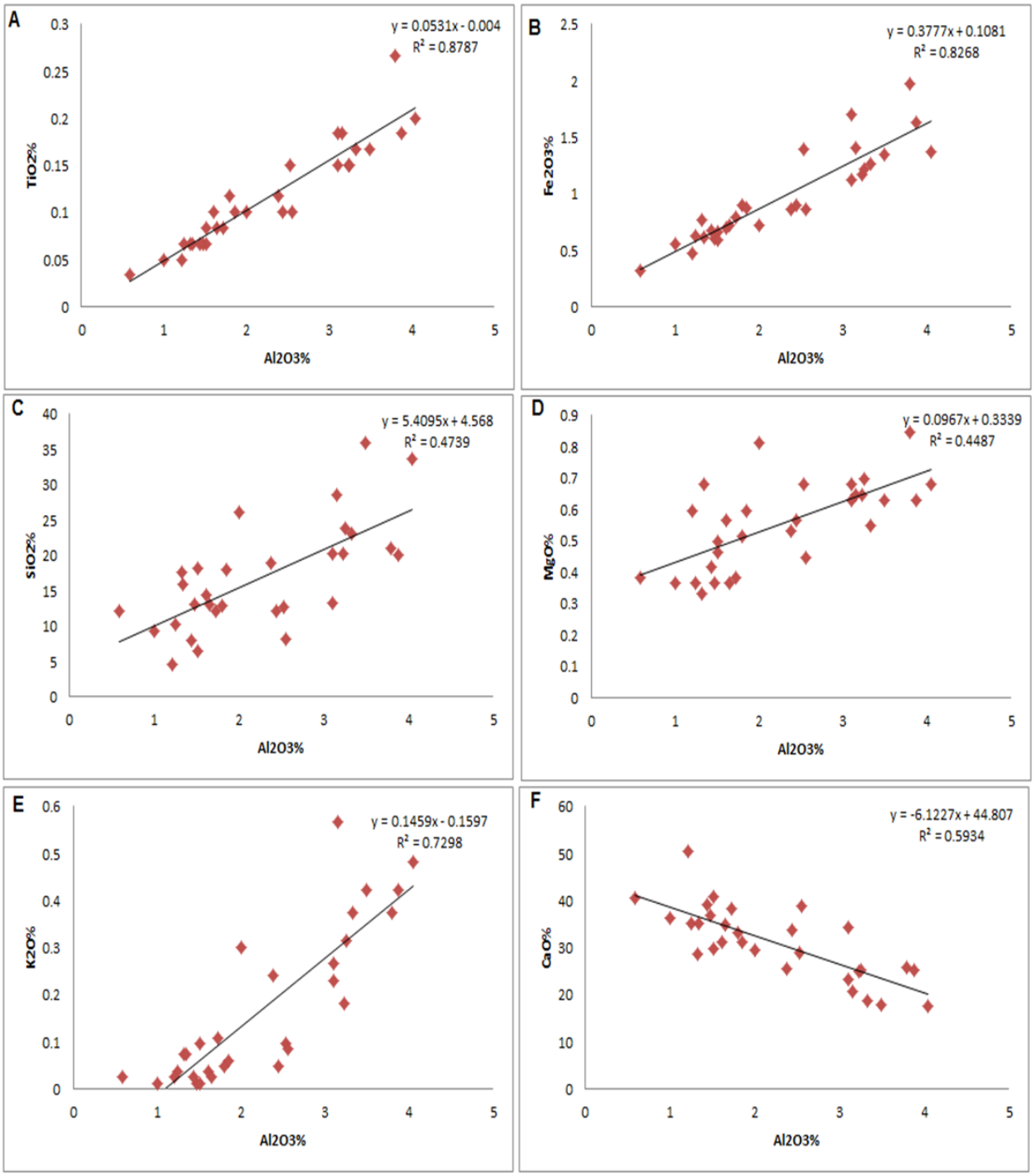

Figure 11. Binary variation diagrams between Al_2O_3 and selected major oxides.

3.4.5 P_2O_5

The average P_2O_5 concentration for samples of the study area is 2.12% (Table 2). As it can be noted in Table 3**Error! Reference source not found.**, the AUG oil shale samples of this study has lowest average P_2O_5 content compared with the oil shale from elsewhere in Jordan. It is attributed to presence of phosphatic rich intervals increase with depth normally close to the contact with the lower phosphate rich formation. Among the trace elements the highest correlation coefficient between P_2O_5 is notices with U (r=0.41) followed by V (r=0.25) (Figure 7), which might occur as trace elements within the apatite crystal structure.

3.4.6 Fe_2O_3

The average Fe_2O_3 is 0.96% (Table 2), which is lower than that reported for Sultani and Al Lajjun (Table 3). As stated earlier in the cluster diagram Fe_2O_3 exhibits almost the strongest similarity with TiO_2 followed by Fe_2O_3-TiO_2 with Al_2O_3 (Figure 5). Furthermore, the correlation coefficient matrix in Figure 6 reveals to the significant positive correlation between Fe_2O_3 and TiO_2 (r = 0.968) and with Cr (r = 0.85), also good correlation between Fe_2O_3-Cu (r = 0.79), Fe_2O_3-MgO (r = 0.66), and Fe_2O_3-Mn (r = 0.65). Iron is present either in the structure of clay minerals and/or as an independent Fe-mineral such as hematite, limonite, and goethite. Iron present in the oil shale may bound to marcasite sulfur or pyrite, also to siderite [22], [31].

3.4.7 MgO

The average MgO in the studied oil shale samples is 0.55%. MgO shows a negative correlation with CaO (r = -0.48). Mg^{2+} may substitute Ca^{2+} in early formed calcite in the form of dolomite and ferroan dolomite; this may reflect the source of both elements [42]. Core logging indicate presence of one or more of dolomite seams interbedded within the oil shale layers. [21] have also reported the presence of MgO in the oil shale attributed to dolomite beds interbed. As in Figure 6, MgO shows a positive correlation with Al_2O_3, SiO_2, K_2O, TiO_2 and Fe_2O_3 (r = 0.67, 0.55, 0.64, 0.72 and 0.66 respectively). MgO may be present in the clay minerals. Mg^{2+} and Ca^{2+} substitute Al^{3+} in the smectite or illite [51]. Na^+ and Mg^{2+} ions are the major exchange cations in marine smectite. Dolomite and clay minerals were detected by XRD analysis in some of the studied oil shale samples.

3.4.8 Na_2O and K_2O

Average Na_2O and K_2O is 0.29% and 0.17% respectively. Vertical variations in the Na_2O and K_2O are narrow. Usually, they are limited to intervals characterized by high Al_2O_3 which may imply presences of smectite clays. However, presence of Na_2O in the form of water-soluble salts mainly halite cannot be ruled out. In general, smectite clays are abundant in oil shale. This is supported by the positive correlation found between K_2O-Na_2O (r= 0.72), K_2O-Al_2O_3 (r =0.85) and Na_2O- SiO_2 (r = 0.7). And supported by the scatter diagram in Figure 12E which suggest there is a positive linear relationship between K_2O and Al_2O_3. The correlation coefficient between each of the Na_2O and K_2O with the other major and trace elements is shown in Figure 6.

3.4.9 TiO_2

The oil shale has low TiO_2 content with an average of 0.12% which similar to what was reported in Sultani and Al Lajjun areas. Geochemistry of TiO_2 in the oil shale can be understood from the strong positive correlation of TiO_2 with Al_2O_3, Fe_2O_3, K_2O and MgO (correlation coefficient r=0.94, 0.97, 0.83, and 0.72 respectively, also strong negative correlation with CaO (r= -0.75). Also, the good correlation between TiO_2-Cr(r=0.86), and TiO_2-Cu (r=0.72). All of these indicate that TiO_2 is essentially associated with clays and reflecting its terrigenous origin, TiO_2 is usually spread within the clays as individual minerals, possibly as rutile, ilmenite, brookite, and anatase [25].

3.5 Geochemistry of trace elements

The results of trace elements of the oil shale for the studied samples from the AUG deposits are given in part per million (ppm) in Table 2.

3.5.1 Zn, V, Ni and Cu

The samples has high Zn, V and Ni content with averages of 1105, 390 and 235 ppm respectively. These averages are higher than the other localities in Table 3. The positive correlation among these elements (r = 0.66 Zn-V, r = 0.66 Zn-Ni, r = 0.68 Zn-Cu) may be explained by their close association with respect to

mineralogy and origin. This positive correlation as related to adsorption on organic matter, clay minerals and Fe-Mg oxides was explained earlier. According to El-Hasan [23] this may indicate that they are more likely to be of authigenic origin and were precipitated, as sulfides, rather than adsorbed by the organic matter. Positive correlation between these trace elements and SO_3 is evident in Figure 6 and supported with the cluster dendrogram in Figure 5 which indicates occurrences in the phosphate-sulfide group. This is except for of Cu which incorporated in the aluminosilicate group (Figure 5). In addition, Zn can replace cations which have bivalent ion such as Ca, Mg and Fe to produce aragonite or calcite. This result is confirmed by the variation diagram in Figure 9C and the correlation matrix in Figure 6 which exhibits the negative correlation coefficient between Zn and CaO (r = -0.57) [26]. The samples probably contain smithsonite (zinc carbonate), probably found in the study area to explain the very high content of Zn in the oil shale samples. The smithsonite is deposited by replacement of limestone.

3.5.2 Sr

Sr is abundant in the studied oil shale samples. The average Sr is 786 ppm, which is two times higher than the crustal average of Sr (384 ppm) [33]. The close association between CaO and Sr is evident from the dendrogram in Figure 5, the correlation coefficient matrix in Figure 6, and from the variation diagram in Figure 9D. Sr may be concentrated by non-calcareous plankton [34], and especially aragonitic materials [26]. Strontianite ($SrCO_3$) mineral have similar structure to calcite and aragonite [25].

3.5.3 Cr

The average Cr is 406 ppm which is higher than the average Cr content in the Sultani oil shale but lower than average Cr in Al Lajjun oil shale. Cr exhibits good positive correlation with oxides such as: TiO_2, Fe_2O_3 and Al_2O_3 (r=0.86, 0.85 and 0.83 respectively). In the dendrogram in Figure 5, Cr is clustered in the aluminosilicate group. Cr showed positive correlation with Ni (r = 0.66). Cr may occur in several forms. It can be adsorbed on iron and manganese oxides, clays, apatite and organic matter [35]. The presence of chromium-bearing minerals in central Jordan has been already reported [37], [38]. The former recorded the presence of chromatite in bituminous phosphatic layers, meanwhile the later reported presence of iron-free volkonskoite smectite clay with 16% Cr_2O_3 occurs in the lower part of the marble zone in central Jordan filling cavities and in veinlets.

3.5.4 Uranium

Uranium attains an average concentration of 21 ppm, which is lower than that in Sultani oil shale and Al Lajjun oil shale. The correlation matrix in Figure 6 indicate that U is positively correlated with most of the major oxides except with CaO. This might be related to the occurrences of U as replacement of Ca inside Ca-bearing primary minerals within the oil shale such as apatite and calcite. In addition, Ca-U oxides (calcium urinates) from central Jordan were identified [38]. Based on the dendrogram shown in Figure 5 and the correlation matrix in Figure 6, the established positive correlation between U and each of V, Cr, Ni, Zn and Zr is most probably due to association inside the phosphate-sulfide group. Secondary uranyl vanadates, carnotite together with volkonskoite are hosted in marble and chalk marl in central Jordan [39].

3.6 Origin of Trace Elements

As can be concluded from the previous sections, the oil shale exhibits significant enrichment in the trace elements including the heavy metals: Zn, Cr, V, and Ni, when compared with other carbonates. The positive correlation between these trace elements and SO_3 is evident. This is supported by the cluster diagram which indicates occurrences mostly in the phosphate-sulfide group. Therefore, the enrichment of these elements cannot be explained only by being incorporated within the organic matter. Or explained only as related to adsorption on clay minerals and Fe-Mg oxides. They are rather the results of the euxinic depositional

environment, where they would co-precipitate as sulfide as indicated by [38] in Al Lajjun area. According to [40], these heavy metals are redox sensitive elements and are related to Mississippi Valley-type deposits.

4. Conclusions

Oil shale core samples were obtained from seven drilled boreholes. The samples have been subjected to thorough investigation including petrographic study, SEM, XRD, and XRF. The geochemical data were evaluated using statistical method to generate scatter plots, correlation matrix and cluster analysis.

The oil shale samples are made of different types of clasts embedded in organic matter-rich carbonate matrix and calcite cement. They consist of bioclastic mudstone-wackestone, bioclastic packstone and foraminiferal grainstone. Based on SEM it was concluded that the carbonate phase in form of calcite is predominant phase followed by silica. The organic matter rich matrix is abundant with dark tones and massive texture. The EDX analysis illustrate that the chemical composition is dominated by calcite, free silica and sulfur compounds.

The XRD results for representative oil shale samples indicate that mineralogy of the AUG oil shale, as a whole, is uniform with depth, and consists of calcite, silica as quartz, phosphates as apatite, and minor amounts of clay minerals and dolomite. The cluster analysis subdivided the elements into three group which are carbonate group; aluminosilicate group; and phosphate-sulfide group. The correlation coefficient matrix and binary diagram plots confirmed the elemental associations. XRF results indicated that CaO is the highest major oxide followed by SiO_2.

The oil shale comprises subordinate and similar average content of SO_3, Al_2O_3 and P_2O_3 (about 2.4 ±0.3 %). XRF results indicate that the oil shale is enriched with trace elements in the study area.

The trace elements concentrations in the order of decreasing abundance of Zn, Sr, Cr, V, Ni, Cu, Zr, Rb, Mn, Ba, U, Y and Th. It was concluded that the enrichment is the result of the euxinic depositional environment, where they would co-precipitate mainly as sulfide minerals. The heavy metals in the oil shale are redox sensitive elements and are related to Mississippi Valley-type deposits.

Funding: This research was funded by the Deanship of Scientific Research - the Hashemite University through the project entitled “Geological and geochemical characterization of oil shale resources in Jordan”.

Acknowledgments: A huge thanks is due to Al-Qamer for Energy & Infrastructure Ltd Company for providing samples from the drilled boreholes in the study area. In addition, earnest thanks are to Jordan Atomic Energy Commission for the support in XRF analysis, Hashemite University and University of Jordan for providing lab facilities and instrumentations. A special thanks is also extended to the anonymous reviewers of this article for their critical comments and suggestions.

5. REFERENCES

[1] A. C. Hutton, “Fluorescence microscopy in oil shale and coal studies, Luminescence microscopy: qualitative and quantitative applications”. Society for Sedimentary Geology 1991, pp. 107-116.

[2] J. R. Dyni, “Oil shale developments in the United States”, Oil Shale, Vol 23, 2006, pp. 7–98.

[3] K. M. Ibrahim, J. O. Jaber, “Geochemistry and environmental impacts of retorted oil shale from Jordan”, Environmental Geology, Vol 52, 2007, pp. 979–984.

[4] M. Voolma, A. Soesoo, V. Puura, S. Hade, H. Aosaar, "Assessing the geochemical variability of oil shale in the Attarat Um Ghudran deposit, Jordan", Estonian Journal of Earth Sciences, Vol 65, 2016, pp. 61–74.

[5] J. Alali, A. Abu Salah, S. Yasin, W. Al Omari, "Mineral status and future opportunity of oil shale", Ministry of Energy and Mineral Resources, Amman, Jordan, Technical Report, 2015.

[6] M. Ali Hussein, M. Alqudah, S. van den Boorn, S. Kolonic, O. G., Podlaha, J. Mutterlose, "Eocene oil shales from Jordan -their petrography, carbon and oxygen stable isotopes", GeoArabia, Vol 19, 2014; pp. 139-162.

[7] V. Puura, A. Soesoo, M. Voolma, S. Hade, H. Aosaar, "Chemical composition of the mineral matter of the Attarat Um Ghudran oil shale, Central Jordan" Oil Shale, Vol 33, 2016, pp. 18–30.

[8] J. H. Powell, B. K. Moh'd, "Evolution of Cretaceous to Eocene alluvial and carbonate platform sequences in central and south Jordan", GeoArabia, Vol 16, 2011, pp. 29-82.

[9] K. M. Ibrahim, B. K. Moh'd, A. I. Masri, M. M. Al-Taj, S. M. Musleh, K. A. Alzughoul, "Volcanotectonic evolution of central Jordan: Evidence from the Shihan volcano", J. Afr. Earth Sci., Vol 100, 2014, pp. 541–553.

[10] J. O. Jaber, A. Amri, K. Ibrahim, "Experimental investigation of effects of oil shale composition on its calorific value and oil yield" Int. J. Oil, Gas and Coal Technology, Vol 4, 2011, pp. 307–321.

[11] V. Puura, A. Soesoo, M. Voolma, M. Konsa, H. Aosaar, "Petrography and mineralogy of the Attarat Um Ghudran oil shale, Central Jordan". Oil Shale, Vol 34, 2017, pp. 110–128.

[12] K. M. Ibrahim, S. Aljurf, H. A. Rahman, C. Gülamber, "Exploration and evaluation of oil shale resources from Attarat area, central Jordan". IMCET 2019, Antalya, Turkey, 16 – 19 April 2019, pp. 1116-1128.

[13] C. Gülamber, K. M. Ibrahim, S. Aljurf, H. A. Rahman, "Introduction of analytical methods for oil shale resource evaluation". IMCET 2019, Antalya, Turkey, 16 – 19 April 2019, pp. 1154-1168.

[14] R.L. Folk, "Petrology of Sedimentary Rock". Hemphill Publishing Company, Austin, United States of America, 1980.

[15] R.J. Dunham, "Classification of carbonate rocks according to their depositional texture". In Classification of Carbonate Rocks, W. E. Ham, ed., A Symposium AAPG Memoir, Tulsa, pp. 108-121.

[16] J.L. Wilson, "Carbonate Facies in Geologic History", Springer-Verlag, New York, 1975.

[17] E. Flügel, "Microfacies of Carbonate Rocks: Analysis, Interpretation and Application", 2nd ed. Springer-Verlag, Berlin, 2010.

[18] U. Brand, J. O. Morrison, I. T. Campbell, "Strontium in sedimentary rocks". In: Geochemistry, Encyclopedia of Earth Science. Springer, Dordrecht, 1998.

[19] J. Lucas, E. El Faleh, L. Prevot, "Experimental study of the substitution of Ca by Sr and Ba in synthetic apatite". Geological Society, London, Special Publications, Vol 52, 1990, pp. 33-47.

[20] Y. Tang, C. Zeiner, C. Santelli, C. Hansel, "Fungal oxidative dissolution of the Mn(ii)-bearing mineral rhodochrosite and the role of metabolites in manganese oxide formation". Environ Microbiol, Vol 15, 2013 pp. 1063-77.

[21] W. Yu, T. J. Algeo, Y. Du, B. Maynard, H. Guo, Q. Zhou, T. Peng, P. Wang, L. Yuan, "Genesis of cryogenian datangpo manganese deposit: Hydrothermal influence and episodic post-glacial ventilation of Nanhua Basin, South China". Palaeogeography, Palaeoclimatology, Palaeoecology, Vol 459, 2016, pp. 321-337.

[22] X. Fu, J. Wang, Y. Zeng, J. Cheng, F. Tan, "Elements in marine oil shale from the Shengli river area, northern Tibet, China", Oil Shale, Vol 28, 2011, pp. 487–506

[23] T. El-Hasan, "Geochemistry of redox-sensitive trace elements and its implication on the mode of formation of the Upper Cretaceous oil shales, Central Jordan", Neues Jahrbuch für Geologie und Paläontologie Abhandlungen, Vol 249, 2008, pp. 333-344.

[24] Y. Hamarneh, "Oil shale resources development in Jordan", Ministry of Energy and Mineral Resources, Natural Resources Authority, Amman. 1998.

[25] J. W Morse, F. T. Mackenzie, "Geochemistry of Sedimentary Carbonates", Elsevier, Amsterdam, 1990.

[26] M. G. Temraz, "Mineralogical and Geochemical Studies of Carbonaceous Shale Deposits from Egypt", Ph.D. Thesis, Technical University of Berlin, Germany, 2005.

[27] A. A. Refaat, "Facies Development of the Coniacian-Santonian Sediments along the Gulf of Suez, Egypt", Ph.D. Thesis, Technical University of Berlin, Germany, 1993.

[28] D. C. Bain, B. F. L. Smith, "Chemical Analysis", In A Handbook of Determinative Methods in Clay Mineralogy, Wilson, M. J. eds., Blackie, Glasgow, pp. 248–274.

[29] J. G. Speight, "Shale Oil Shale Production Process", 1st ed., Gulf Professional Printing, Elsevier, 2019.

[30] A. M. Abed, K. Arouri, B. S. Amireh, Z. Al-Hawari, "Characterization and genesis of some Jordanian oil shales", Dirasat, Vol 36, 2009, pp. 7-17.

[31] A. Ots, "Estonian oil shale properties and utilization in power plants", Energetika, Vol 53, 2007, pp. 8–18.

[32] C.E. Weaver, L. D. Pollard, "The Chemistry of Clay Minerals", Elsevier, Amsterdam, 1973.

[33] Sr – Strontium, pp. 374-352, http://weppi.gtk.fi/publ/foregsatlas/text/Sr.pdf (accessed on 22 December 2022)

[34] G. A. Knauer, J. H. Martin, “Seasonal variation of Cd, Co, Mn, Pb ad Zn in water and phytoplankton in Monterey bay, California”, Limnol. Oceanogr. Milwaukee, Vol 18, 1973, pp. 597- 604.

[35] L. Prevot, “Geochemistry, Petrography, Genesis of Cretaceous-Eocene Phosphorites, the Ganntour Deposit (Morocco): a type example”. Ph.D. Thesis, University Louis Pasteur, Strasbourg, 1990.

[36] W. Heimbach, “Zum Vorkommen von Chromatit, CaCrO, in Jordanien”, Geol. Jb., Vol 83, 1965, pp. 717-724.

[37] H. N. Khoury, R. C. Mackenzie, J. D. Russell, J. M. Tait, “An iron-free volkonskoite” Clay Minerals, Vol 19, 1984; pp. 43 – 57.

[38] H. Khoury, E. Sokol, I. D. Clark, “Calcium uranium oxides from central Jordan: associations, chemistry, and alteration products”, Canadian Mineralogist, Vol 53, 2015, pp. 1-22.

[39] H. Khoury, “Uranium minerals of central Jordan”, Applied Earth Science IMM Transactions, section B, Vol 124, 2015, pp. 104-128.

[40] K. M. Ibrahim, S. Aljurf, J. Abu Hawas, “Metal sulphides associated with Attarat oil shale, Jordan”, 2nd International Oil Shale Conference (BAU-SIOSC), 9-11October 2018, As Salt- Jordan.